Available online at www.sciencedirect.com

ScienceDirect

Solar Energy 115 (2015) 777–790

SOLAR ENERGY

www.elsevier.com/locate/solener

Using remote sensing to quantify albedo of roofs in seven California cities, Part 1: Methods

George A. Ban-Weiss [a,b,*], Jordan Woods [b], Ronnen Levinson [b]

[a] Dept of Civil and Environmental Engineering, University of Southern California, 3620 Vermont Ave KAP210, Los Angeles, CA 90089, United States
[b] Heat Island Group, Lawrence Berkeley National Laboratory, One Cyclotron Road, Berkeley, CA 94720, United States

Received 17 July 2014; received in revised form 8 October 2014; accepted 9 October 2014
Available online 15 December 2014

Communicated by: Associate Editor Matheos Santamouris

Abstract

Cool roofs reflect sunlight and therefore can reduce cooling energy use in buildings. Further, since roofs typically cover about 20–25% of a city, widespread deployment of cool roofs could mitigate the urban heat island effect and partially counter urban temperature increases associated with global scale climate change. The magnitude of these potential benefits for a given city depends on the increase in albedo that can be achieved using reflective roofs. Assessing this increase requires knowledge of roof albedo at the city scale, which until now has been hindered by a lack of reflectance data with sufficient spatial coverage, spatial resolution, and spectral detail. In this work we use multiband aerial imagery to derive the albedos of individual roofs in seven California cities: Los Angeles, Long Beach, San Diego, Bakersfield, Sacramento, San Francisco, and San Jose. The radiometrically calibrated, remotely sensed imagery has high spatial resolution (1 m) and four narrowband reflectances: blue, green, red, and near-infrared. First, we locate roof pixels within GIS building outlines. Next, we use laboratory measurements of the solar spectral reflectances of 190 roofing products to empirically relate broadband solar reflectance to reflectances in the four narrow bands; this empirical relationship well predicts solar reflectance, as indicated by a low root-mean-square of the residuals of 0.016. Albedos computed from remotely sensed reflectances are calibrated to ground measurements of roof albedo in each city. The error (accuracy) at 90% confidence interval of the calibrated albedos is found to vary by city, from 0.00–0.01 at low albedo and 0.06–0.14 at high albedo.

Keywords: Albedo; Solar reflectance; Cool roof; Heat island effect

1. Introduction

Roofs cover the tops of buildings, separating the atmosphere from the indoor environment. The solar reflectance or "albedo" of a rooftop is the fraction of incident solar energy that is reflected. Sunlight that is not reflected is instead absorbed by the roof; this energy is then transferred to the interior of the building and to the atmosphere. Dark roofs can have albedos as low as 0.05, meaning that they can absorb up to 95% of incident sunlight. Clean bright white roofs can have albedos above 0.90 (CRRC, 2013), reflecting nearly all incident sunlight.

Monitoring studies have shown that replacing a dark roof with a white roof can decrease heat flows into the conditioned space, and lower cooling energy use. In many cases, cooling energy use reductions of 10–20% have been observed (Parker et al., 1995, 1998; Akbari et al., 1997,

* Corresponding author at: Dept of Civil and Environmental Engineering, University of Southern California, 3620 Vermont Ave KAP210, Los Angeles, CA 90089, United States. Tel.: +1 213 740 9124; fax: +1 213 744 1426.
E-mail address: banweiss@usc.edu (G.A. Ban-Weiss).

http://dx.doi.org/10.1016/j.solener.2014.10.022
0038-092X/

2001, 2005; Konopacki and Akbari, 2001; Akbari, 2003). The cooling energy savings attainable for a particular building depends on its construction, roof and attic insulation, shade cover, and climate. In some situations, such as when roofs are thermally decoupled from the conditioned space, reflective roofs can have negligible effect on energy use (Ban-Weiss et al., 2013). Recognizing the potential energy and cost savings of white roofs, in October 2005 the California Energy Commission added to its Title 24 Building Energy Efficiency Standards (CEC, 2005) a prescription that new or retrofitted low-sloped roofs on commercial buildings should generally be white. When the costs of white and dark roofs are approximately the same, reductions in energy costs translate directly to money saved. Note that while reflective roofs can increase heating energy use requirements in the winter, summer cooling cost savings in most of California's climate zones far outweigh this winter heating cost penalty (Levinson and Akbari, 2010).

Solar reflective roofs have lower surface temperatures and thus transfer less heat to the atmosphere than dark roofs. In most cases this reduced heat flow lowers surrounding air temperatures. An observational study (Campra et al., 2008) showed that from 1983 to 2006, a region of southeastern Spain experienced near-surface air temperature decreases of about 0.3 °C/decade as greenhouses with high albedo roofs were deployed. Since roofs on average comprise about 20–25% of surface areas in North American cities (Akbari et al., 1999, 2003; Akbari and Rose, 2001a,b, 2008; Rose et al., 2003), large-scale deployment of white roofs has been suggested as a measure to mitigate the urban heat island effect (Taha et al., 1988; Akbari et al., 1990, 1992; Rosenfeld et al., 1995). Similarly, reflective roofs may lessen urban temperature increases associated with global scale climate change. A remote sensing study (Mackey et al. 2012) found that use of cool roofs in Chicago for reducing urban heat islands has increased city-wide albedo and decreased roof surface temperatures as detected by the LANDSAT satellite. Various mesoscale climate modeling studies have simulated the climate effects of hypothetical increases in urban albedo. For example, simulations reported by Taha (2008a) found 1–2 °C decreases in peak urban temperatures at six locations in California. Other studies have shown comparable temperature reductions in other regions (Synnefa et al., 2008; Taha, 2008b; Lynn et al., 2009; Zhou and Shepherd, 2009). We note that one study showed that in some situations urban air temperatures can rise with increased urban albedo (Taha, 2008c); this study hypothesized that the modeled temperature increase in Houston, Texas was due to reduction of the atmospheric mixing height.

Other modeling studies have investigated the effects of increasing urban albedo across the United States (Millstein and Menon, 2011) and globally (Akbari et al., 2009, 2012; Menon et al., 2010; Oleson et al., 2010; Jacobson and Ten Hoeve, 2012; Akbari and Matthews, 2012; Cotana et al., 2014). Millstein and Menon (2011) used a regional climate model to show that adopting cool roofs and pavements in urban areas of the United States could reduce afternoon summertime temperatures in urban locations by 0.1–0.5 °C. A study using a global climate model (Oleson et al., 2010) demonstrated that reflective surfaces could decrease the annual mean urban heat island effect[1] to 0.8 °C from 1.2 °C.

While reflective surfaces have been modeled in most situations to reduce urban temperatures, their effects on the hydrological cycle also warrants investigation. One mesoscale climate modeling study (Georgescu et al., 2012) has suggested that reflective surfaces may reduce precipitation around Phoenix, Arizona. Since Phoenix has unique desert meteorology with most of its precipitation arriving with late-summer monsoon thunderstorms, this result may not hold in other regions.

Determining realistic estimates of the potential for increasing roof albedo at the city scale requires detailed understanding of the current stock of roofs. Currently there are no estimates of city-wide mean roof albedos. There are at least five challenges associated with quantifying roof albedo at the city scale: spatial coverage, spatial resolution, spectral coverage, radiometric calibration, and cost. For example, roof albedo can be accurately measured at the rooftop by using a pyranometer to measure incident and reflected (bihemispherical) sunlight (ASTM, 2010). However, measuring a sample large enough to statistically represent the roofs of a city is logistically prohibitive. Remote sensing can rapidly characterize large geographic areas. For example, there exist freely available surface albedo datasets derived from satellite sensors like MODIS (Schaaf et al., 2002; Schaaf, 2004). Data are available describing both directional-hemispherical reflectance (referred to as "black-sky" albedo) and bihemispherical reflectance (referred to as white-sky albedo). However, its spatial resolution of 500 m (16-day composites) is too low to distinguish various urban surface types such as roofs. Imagery from commercial satellites (e.g., GeoEye, IKONOS) offers spatial resolutions on the order of 1 m and spectral detail at visible and near-infrared (near-IR) wavelengths. While the spatial resolution and spectral detail may be sufficient to distinguish roofs and compute roof albedo, purchasing these imagery for entire cities would be costly. As of 2014, minimum costs for these data are roughly US$15 per km^2, so acquiring imagery for only the City of Los Angeles would be about $20,000, and for the entire metropolitan area of Los Angeles about $200,000. Another option is aerial imagery, which is often acquired from aircraft. Since these aircraft are generally nearer to the ground than satellites, the captured imagery is at higher spatial resolution. While aerial imagery can sometimes provide multiband information in the visible and near IR, it is almost always acquired for generating

[1] The urban heat island effect was defined by Oleson et al. (2010) as the difference (urban – non-urban) in 2-m air temperature between urban and non-urban portions of model grid cells.

photographs, and therefore does not provide the calibrated radiance data needed for scientific analysis. To overcome the aforementioned challenges associated with spatial coverage of ground measurements, cost and spatial resolution of satellite data, and radiometric limitations of most aerial imagery, we acquired high-resolution, radiometrically calibrated, aerial imagery for the purpose of deriving roof albedos.

In this paper we develop a method for using radiometrically calibrated aerial imagery to estimate roof albedos for seven cities in California: Los Angeles, Long Beach, San Diego, Bakersfield, Sacramento, San Francisco, and San Jose. The aerial imagery has high spatial resolution (1 m) and includes reflectances in four narrow spectral bands: three in the visible spectrum (blue, green, and red), and one in the near-infrared spectrum. The near-IR contains approximately 50% of the energy from the sun (Levinson et al., 2010). Some "cool roofs" have low reflectance in the visible spectrum but high reflectance in the near-IR spectrum, allowing the roof to remain dark while increasing its albedo (Levinson et al., 2007). Thus, having information about reflectance in both the visible and near-IR spectra improves estimates of roof albedo. The work is presented in two parts. In Part 1 (this paper), we present methods for calculating roof albedo from remotely sensed reflectances, and show sample results. Part 2 (a companion paper, Ban-Weiss et al., 2015) reports roof albedos in each of the seven California cities of interest. It also provides further analyses and applications using the albedo dataset. Applications include use of roof albedos in a regional climate model to estimate temperature decreases attainable by converting the current stock of roofs to solar reflective cool roofs. This work is a first attempt to quantify the albedos of individual roofs at the scale of entire cities.

2. Methods

In this section we describe the methods developed to derive the albedos of roofs in seven California cities: Los Angeles, Long Beach, San Diego, Bakersfield, Sacramento, San Francisco, and San Jose. Fig. 1 diagrams the approach. Reflectances in narrow bands denoted blue, green, red, and near-IR were obtained from high spatial resolution (1 m) imagery acquired using airplanes during summer 2009. We refer to the data collected using the airplane as "remotely sensed." Pixels containing roofs were then extracted from the imagery. Roof pixels were identified using geographic information system (GIS) building outline datasets for entire cities where available. When building outline datasets were not available, manual tracing of buildings was performed. Laboratory measurements of the solar spectral reflectances of 190 roofing products were used to empirically relate solar reflectance to reflectances in the four narrow bands. Remotely sensed solar reflectances were calibrated to ground measurements of roof albedo in each city. Pixels within each roof boundary were then averaged to calculate the mean albedo of each roof. Note that we define albedo consistently with the "cool roof" scientific community as the ratio of reflected to incident broadband solar radiation, and subsequently specify the illumination-viewing geometry for each measurement. Each step is now described in more detail.

2.1. Data source

The aerial imagery was originally acquired for the National Agriculture Imagery Program (NAIP), which is administered by the US Department of Agriculture (USDA). NAIP annually collects aerial imagery during the agricultural growing season (late spring to early

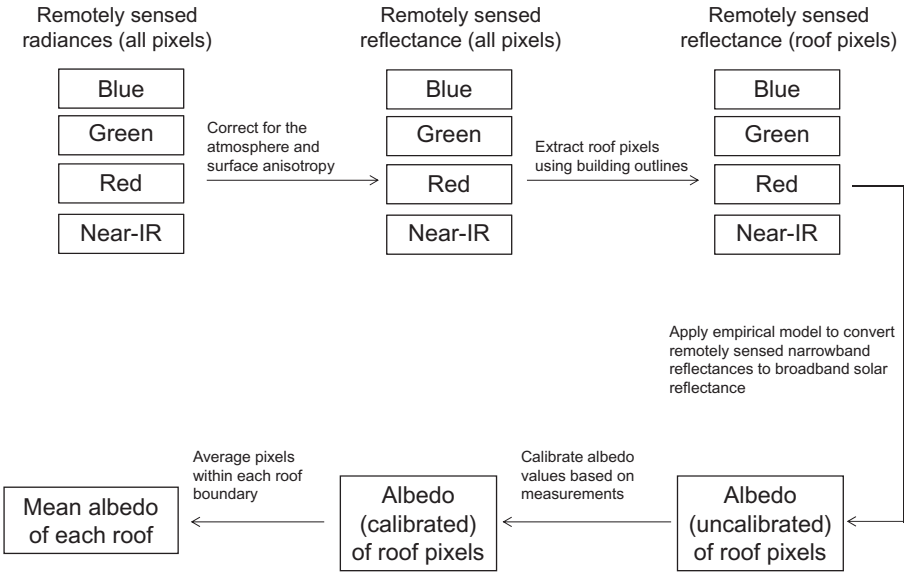

Fig. 1. Schematic of our approach for computing the mean albedo of individual roofs from the aerial imagery.

summer) in the continental United States. One of the main goals of NAIP is to provide digital ortho photography to government agencies and the public. While this program is focused on agriculture, imagery is generally acquired for entire states including urban areas. NAIP has strict requirements to ensure high image quality. For example, to minimize shadows, flights must occur when the sun is at least 30° above the horizon. In practice, all imagery is collected when the sun is at least 60° above the horizon. Flights must acquire imagery on clear days without cloud cover (NAIP, 2013).

NAIP imagery is available for the entire state of California at 1 m spatial resolution in years 2005, 2009, 2010, and 2012 (NAIP, 2013). NAIP contracts different companies to acquire imagery each year. As such, various imagery acquisition systems have been used. In 2009, imagery for California was collected by North West Group (Calgary, Alberta, Canada) using a Leica ADS80/SH82 airborne digital sensor (Leica, 2013). This sensor is more than a high-speed digital camera for photography. It utilizes arrays of digital charge-coupled devices that sense light in four narrow spectral bands (blue, 420–492 nm; green, 533–587 nm; red, 604–664 nm; and near-IR, 833–920 nm). The arrays of detectors are arranged perpendicular to the flight direction in a "push broom" configuration. Each detector is radiometrically calibrated in the laboratory to accurately measure radiance in its spectral band. Thus, the sensor accurately measures multi-spectral radiance, similar to that acquired by sensors on satellites for scientific applications. In this way, the imagery collected by the sensor has the potential to be used as a scientific remote sensing data set, rather than simply as photographs. NAIP imagery is publically available as either "digital ortho quarter quads" (DOQQs) or "compressed county mosaics" (CCMs); both options include imagery compression, a variety of color adjustments, and other post-processing required by NAIP (NAIP, 2013). This post-processing improves the overall appearance and usability of the imagery, but destroys the radiometric calibration, which is important for the purposes of this study. Therefore, we acquired directly from NAIP's vendor for 2009 (North West Group) the radiometrically calibrated radiance data for images within our cities of interest. The field of view of the sensor resulted in image footprints that are 12 km wide (perpendicular to flight direction), and of varying length depending on flight paths. The mean altitude of the flights was about 9 km above ground level, leading to view zenith angles for the line scanner up to about 34°. Each flight strip has 15% overlap with the adjacent flight strip corresponding to view zenith angles of 30–34°; thus, about 30% of the area for each city has duplicate imagery.

2.2. Correcting for the atmosphere and surface reflectance anisotropy

Since we are interested in reflectance at Earth's surface, the radiance measurements at the sensor (on the airplane) need to be corrected for atmospheric scattering and for surface reflectance anisotropy. Techniques have been previously developed and described at length elsewhere, so we provide only a brief description here.

Atmospheric gases and particles can influence the perceived "at-sensor" radiance through multiple pathways (Schaepman-Strub et al., 2006; Downey et al., 2010). The atmospheric correction allows for estimating surface reflectance by isolating (a) the radiance that originates from the Earth surface, and (b) the solar spectral irradiance at the surface. The surface spectral reflectance, a characteristic of the coupled surface-atmosphere system, is a function of the measured at-sensor radiance, the mean solar spectral irradiance at the top of atmosphere (TOA), the path radiance over an absorbing surface (i.e., the "dark pixel" radiance from downwelling sunlight that is reflected by the atmosphere into the sensor before having reached the surface), the total downward transmittance from the TOA to the ground, the total upward transmittance from the ground to the sensor, and the spherical albedo of the atmosphere (i.e., the fraction of upward radiance that is then backscattered by the atmosphere) (Kaufman and Sendra, 1988; Fraser et al., 1992). The first term, at-sensor radiance, is measured. The second term, TOA mean solar spectral irradiance, can be computed from the solar constant as a function of the cosine of the solar zenith angle. The latter four unknown terms are estimated using a modified Song-Lu-Wesley method (Song et al., 2003, Downey et al., 2000), which is based on a linear parameterization similar to that used by the Advanced Very High Resolution Radiometer (AVHRR) satellite sensor. The atmospheric reflectance for each view and sun zenith angle is first estimated using expected versus measured surface reflectances for dark pixels. The four unknown parameters are then determined for each spectral band based on parameterizations derived from atmospheric modeling performed for various flying heights, ground elevations, sun and view zenith angles, and atmospheric reflectances. Past studies have validated the atmospheric correction by comparing to ground reflectance measurements (Beisl and Adiguezel, 2010; Markelin et al., 2010) and found agreement to within 10%.

The correction accounting for surface reflectance anisotropy is based on a modified Walthall method (Beisl et al., 2008; Downey et al., 2010). Since flights for NAIP are always in the north–south direction, the correction minimizes spurious east–west gradients in reflectance (i.e., those perpendicular to the flight direction). The method is semi-empirical and the sum of "kernels" accounting for incident illumination zenith angle, reflection view zenith angle, relative azimuth angle (Nilson and Kuusk, 1989), and an additional "hot spot" term based on the distance function of the Li-kernels from the AMBRALS model (Wanner et al., 1995). The correction in part uses summary statistics for land pixels at equal viewing zenith angles, and masks water so that specular reflection does not influence results (Downey et al., 2010).

Strictly speaking, the resulting reflectances described here are hemisphere-directional reflectance factors (HDRF), using the naming conventions described by Schaepman-Strub et al. (2006). In this investigation we aim to derive bihemispherical reflectances (BHR). The most physical methods for deriving BHR from HDRF require either knowledge of the Bidirectional Reflectance Distribution Function (BRDF) for each roofing material, or many aerial images for each location at a variety of viewing angles. Because we have neither, we use rooftop measurements of BHR to 'calibrate' HDRFs (see Section 2.5). Such a calibration is justified by the high correlation observed between HDRF and BHR for vegetation canopies, shown in Fig. 4 of Schaepman-Strub et al. (2006). We expect even higher correlation for roofing materials given that their surfaces are generally more isotropic than natural vegetative surfaces. While this simplification contributes to the errors later discussed in Section 3.2 and reported in Table 3, we note that differences between HDRF and BHR are generally small. For example, for vegetation canopies, the absolute difference between these two metrics is <0.02, with relative differences up to 14%, which we deem tolerable for the purposes of our study (Schaepman-Strub et al., 2006). Because of the reduced anisotropy of roofs, differences are expected to be lower for roofs than vegetation. Errors introduced by this simplification are explored in Section 4.2, which compares albedos for buildings with duplicate values computed independently using two different view zenith angles (about $-30°$ versus $+30°$).

Surface reflectances (HDRFs) are reported for each of the four narrow bands in each 1 m pixel; we refer to these as the remotely sensed blue, green, red, and near-infrared reflectances. Fig. 2 shows example imagery for the four narrow bands in a portion of San Jose, California. Low reflectance pixels in each narrow band are dark, and high reflectance pixels are light. (Note that the line of trees on the right side of the image shows higher reflectance in the near-IR than in the red, a characteristic of light reflection from leafs (Slaton et al., 2001).) The remaining subsections describe our derivation of roof albedo (i.e., broadband solar reflectance) from these narrowband reflectances (Fig. 2).

2.3. Extracting roof pixels from the imagery

Next we identify in the imagery pixels containing roofs. For five of the seven cities of interest (Los Angeles, Long Beach, Bakersfield, San Francisco, and San Jose), shapefiles containing outlines for every building within the city were acquired from local governments (Table 1). Example building outlines projected onto a red–green–blue (RGB) composite of the aerial imagery in San Jose are shown in Fig. 3a. The building outlines include detailed features of each building, as can be better observed when projected onto higher spatial resolution (but not radiometrically

Table 1
Sources of shapefiles containing outlines of all buildings within five of the seven cities of focus. Outlines were not available in Sacramento and San Diego.

City	Source
San Jose	City of San Jose (2011)
San Francisco	City and County of San Francisco (2011)
Bakersfield	City of Bakersfield (2011)
City of Los Angeles	Los Angeles Region Imagery Acquisition Consortium 3 (2011)
Long Beach	Los Angeles Region Imagery Acquisition Consortium 3 (2011)

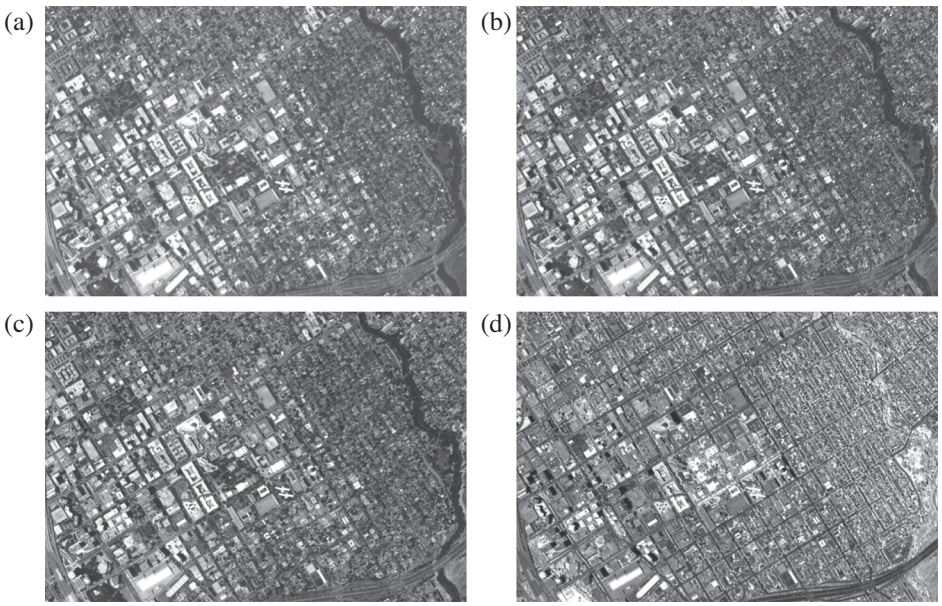

Fig. 2. Examples of the 1 m resolution remotely sensed imagery for a portion of San Jose, California, showing reflectances in four narrow bands: (a) blue (420–492 nm), (b) green (533–587 nm), (c) red (604–664 nm), and (d) near-IR (833–920 nm).

Fig. 3. Examples of building outlines. Outlines provided by the City of San Jose are shown in (a) and (b). Manually traced outlines in Sacramento are in (c). In (a) and (c) the underlying imagery is an RGB composite of the aerial imagery described in this paper. Panel b uses higher-resolution (but not radiometrically calibrated) background imagery from the United States Geological Survey) to better resolve fine features.

calibrated) imagery from United States Geological Survey (USGS) (Fig. 3b). In our analysis we assume that building outlines and roof outlines are colocated.

In the two cities for which we could not acquire building outlines (Sacramento and San Diego), we manually traced the edges of buildings in the imagery using ESRI ArcMap 10.0. Manually tracing perfect outlines proved difficult. We therefore intentionally traced outlines that were slightly within the actual building borders, ensuring that non-roof pixels were not included within the boundaries. Manually tracing every building was not feasible, so we traced a small but statistically representative sample of buildings within each of these two cities. To determine the number of buildings needed to properly characterize the mean roof albedo of a city, we performed a Monte Carlo statistical investigation using the population of albedo values computed for Los Angeles. As shown in our companion paper (Ban-Weiss et al., 2015), a set of 1000 roof outlines was found to be sufficient. Hundreds of 300×300 m quadrats (small, typically rectangular study regions) were generated in random locations within city boundaries; all roofs within the borders of the quadrats were traced until the minimum number of outlines ($N = 1000$) was met. An example of manually traced outlines within a quadrat in Sacramento is shown in Fig. 3c.

2.4. Relating broadband solar reflectance to narrowband reflectances

To quantify roof albedo, we need a method to relate broadband solar reflectance to the four (narrowband) remotely sensed reflectances. In this section we describe this spectral conversion. We note again that we use "albedo" to mean broadband solar reflectance without regard to the angular characteristics of incoming and reflected light; these geometries are instead described for each measurement. (This naming convention is consistent with that of the cool roof scientific community, but is inconsistent with that of the remote sensing community, which reserves albedo to mean bihemispherical reflectance (Schaepman-Strub et al., 2006).) We began by computing the solar, visible, and narrowband (blue, green, red, and near-IR) reflectances of each of 190 roofing products from laboratory measurements of solar spectral reflectance. Included in the 190 samples were all widely used roofing types in California for both commercial and residential buildings (Table 2). Samples were

Table 2
Roofing samples for which we measured solar spectral reflectances in the laboratory.

Roofing product type	Number of samples
Asphalt shingle	75
Concrete tile	25
Clay tile	36
Metal roofing	5
Single-ply membrane	30
Modified bitumen cap sheet	14
Field-applied coating	5
Total	190

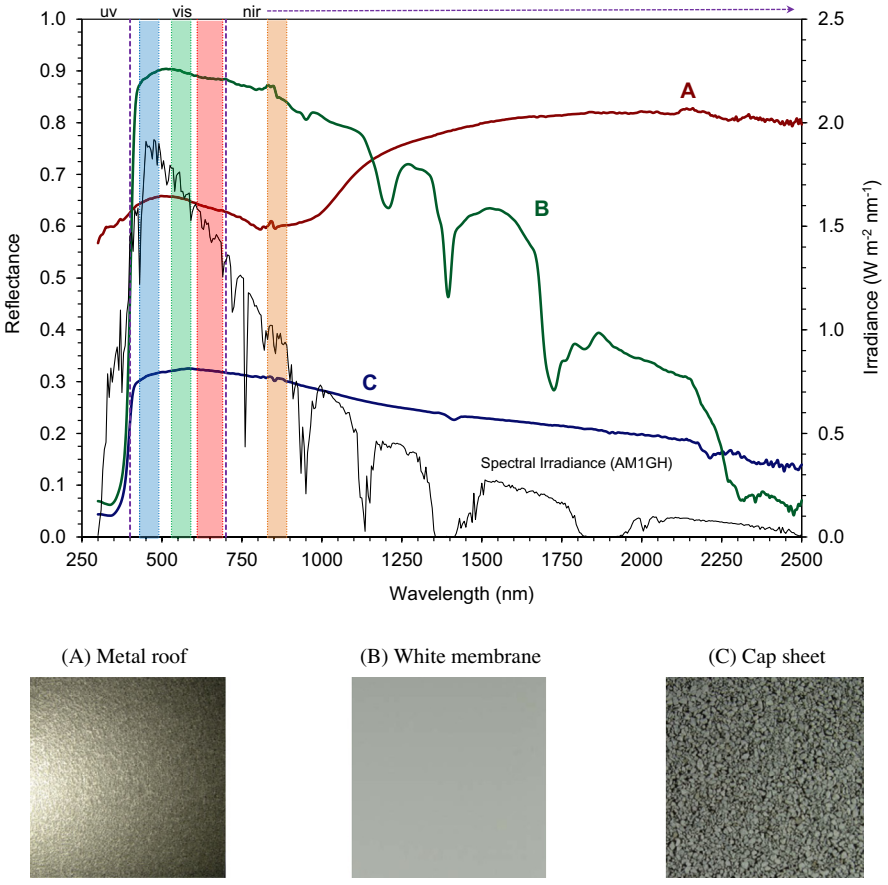

Fig. 4. Solar spectral reflectances of three roofing products: (A) metal (zincalume with clear resin), (B) white membrane, and (C) granule-surfaced modified bitumen cap sheet. Also shown is the solar spectral global horizontal irradiance at Earth's surface (black line) assuming clear sky with the sun at zenith, referred to as Air Mass 1 Global Horizontal (AM1GH). Shaded regions (left to right: blue, green, red, near-IR) show the narrowband spectral ranges sensed by the airborne digital sensor (ADS80/SH82) used to collect the imagery.

new and mostly acquired from various roofing supply stores in the San Francisco Bay area. Clay tile samples were provided by MCA Superior Clay Roofing Tiles. While use of roofing materials that had been aged outdoors was desired, it was infeasible to collect soiled roofing materials. Solar spectral reflectance was measured using a PerkinElmer Lambda 900 UV/Vis/NIR spectrophotometer equipped with a 150-mm Labsphere integrating sphere. Spectral reflectances were measured from 300 to 2500 nm in 5 nm steps. All measurements are of near-normal (8°) beam-hemispherical reflectance (a.k.a. directional-hemispherical reflectance using the naming convention of Schaepman-Strub et al., 2006) following ASTM Standard E903-12.

Fig. 4 shows the solar spectral reflectance, $\rho(\lambda)$, of several roofing products, as well as the solar spectral irradiance, $j(\lambda)$, used to compute band reflectances. This air mass one global horizontal (AM1GH) terrestrial irradiance assumes a clear sky and the sun at zenith, and is suited to characterizing roof solar reflectance (Levinson et al., 2010). Irradiance-weighted band reflectance R over each range of interest was calculated as

$$R = \frac{\int_{\text{range}} j(\lambda)\rho(\lambda)\,d\lambda}{\int_{\text{range}} j(\lambda)\,d\lambda} \quad (1)$$

We computed four narrowband reflectances—blue, b (420–492 nm); green, g (533–587 nm); red, r (604–664 nm); and near-IR, i (833–920 nm)—and three broadband reflectances: visible, V (400–700 nm), near-IR, I (700–2500 nm), and solar, S (300–2500 nm). (Narrowband spectral ranges correspond to those of the remote sensor. Lowercase symbols represent narrowband reflectances and uppercase symbols represent broadband reflectances.) Note that while the narrow blue, green, and red spectra collectively span most of the visible spectrum, the narrow near-infrared spectrum used to compute i spans less than 5% of the full near-infrared spectrum (700–2500 nm) (Fig. 4). Hence, we expect (b, g, r) to predict V more accurately than (b, g, r, i) can predict S.

Using the aforementioned laboratory measurements we developed empirical relationships between broadband and narrowband reflectances using multivariate regression.

We first modeled $V = V(b, g, r)$ to test the method, then modeled $S = S(b, g, r, i)$.

2.5. Calibrating remotely sensed values using ground truths

To calibrate the remotely sensed values, we measured the albedos of several roofs in each city, and then evaluated $S(b, g, r, i)$ for these roofs using remotely sensed b, g, r, and i. Measured albedos were obtained using one of two methods. In the first, we identified buildings that had new roofs installed within six months prior to the flights. The make and model of the new roof was known, allowing us to obtain its albedo from an online database (CRRC, 2013). In the second, we measured rooftop albedos with a pyranometer. The pyranometer measurements were performed in July 2012 in San Jose and Los Angeles, and in September 2012 in San Francisco and Davis (near Sacramento). Since these measurements were taken about three years after the imagery was acquired via airplane, the second method was implemented only for roofs with low measured albedos ($S < 0.4$); as shown in Sleiman et al. (2011), aging (i.e., weathering and soiling) has a small effect on the albedo of such roofs in this range. White roofing products can show marked decreases in albedo after three years (Sleiman et al., 2011) and were therefore not included in this second method.

Method 1 (applied to all roofs): Several roof manufacturers and vendors identified the make and model of roofs installed in each city no more than six months prior to each flight. The initial solar reflectance of each installed roof was then obtained from the Rated Products Directory of the Cool Roof Rating Council (CRRC, 2013). Corresponding remotely sensed albedos were then quantified by randomly sampling 10 pixels within the roof boundary. Only pixels with visible roofing material were included; HVAC equipment, solar photovoltaics, skylights, and other features were excluded. In total, 31 buildings with known installation dates and roofing product types were used.

Method 2 (applied only to roofs with low measured albedo): We measured the albedo of roofs on 10 buildings in (or very near) four of the seven cities using a Kipp & Zonen CMA6 first-class albedometer, which integrates back-to-back a pair of Kipp & Zonen CMP6 first-class pyranometers. In situ roof albedos were measured following ASTM Standard E1918-06, "Standard Test Method for Measuring the Solar Reflectance of Horizontal and Low-Sloped Surfaces in the Field" (ASTM, 2010), which determines bihemispherical solar reflectance with solar beam incidence angle <45°. Three consecutive albedo measurements were performed at each of three locations on each roof, for a total of nine measurements per roof. The mean albedo was calculated by averaging these nine measurements. Corresponding remotely sensed albedos were extracted by identifying each measurement location in the imagery; the mean value of pixels within a 3 m radius was calculated to approximate the field of view of the pyranometer. This was done for each of the three measurement locations per roof. The three resulting albedos were then averaged and compared to the measurement-derived mean albedo for each roof.

We were unable to obtain measurements for low albedo roofs in Bakersfield using either Method 1 or Method 2. Instead, we obtained from Bakersfield Public Works records of asphalt concrete pavement installations. Two roads were paved within one year prior to the flights; installations were 3 weeks and 8 months prior to the flights, respectively. Associated albedos were assumed to be 0.05 and 0.07, respectively, derived from measurements of the post-installation time evolution of asphalt pavement albedo (unpublished). Corresponding remotely sensed values were obtained using the random sampling technique described above for Method 1.

Measured albedo, S_{measured}, was regressed to remotely sensed albedo, $S(b, g, r, i)$, using a power law relationship of the form:

$$S_{\text{measured}} = a_c S^{p_c} \tag{2}$$

This was done separately for each city to determine parameters a_c and p_c, where subscript c indexes the seven cities. These power law parameters were then used to determine the calibrated remotely sensed (pixel level) albedo S' in each city as:

$$S' = a_c S^{p_c} \tag{3}$$

where the prime indicates "calibrated." The error ε (accuracy) of the remotely sensed albedos (S') in each city was then estimated using the standard errors of the power law parameters. Upper and lower-bound estimates of the coefficients were derived as mean value ±90% confidence interval. One-sided confidence intervals above (ε^{U}) and below (ε^{L}) the mean were then calculated as a function of calibrated albedo as:

$$\varepsilon^{\text{U}}(S') = a_c^{\text{U}} S^{p_c^{\text{U}}} - S' \tag{4}$$

$$\varepsilon^{\text{L}}(S') = S' - a_c^{\text{L}} S^{p_c^{\text{L}}} \tag{5}$$

where superscripts U and L correspond to upper- and lower-bound parameter estimates. These error estimates indicate the accuracy with which calibrated albedos are calculated from uncalibrated remotely sensed values. Note that we present one-sided confidence intervals because the power law form of Eq. (3) makes ε asymmetric about S'.

White roofs are commonly single-ply (plastic) membranes or elastomeric coatings, both of which are very smooth and glossy when new. Reflection from these materials can therefore include a non-negligible specular component at high angles of sunlight incidence (see for example Levinson et al., 2010). Since white roofs are almost always low-slope and flights occurred with the sun at least 60° above the horizon, we expect in most cases that the specular component of reflection will be negligible. However, some commercial roofs can be "wavy" and have areas with high pitch, making the incidence angle large and introducing a non-negligible specular reflection.

Table 3
Estimated error ε (accuracy) at 90% confidence interval of the calibrated remotely sensed albedos. ε is shown for each city and for different values of calibrated albedo S'. One-sided confidence intervals are shown because they are asymmetric about the mean; ε^U is the upper and ε^L the lower interval. The City of Los Angeles and Long Beach are shown together since both are part of the Greater Los Angeles Area.

Albedo	Error											
	Los Angeles/Long Beach		Sacramento		San Jose		San Francisco		San Diego		Bakersfield	
	ε^U	ε^L	ε^U	ε^L	ε^U	ε^L	ε^U	ε^L	ε^U	ε^L	ε^U	ε^L
0.1	0.00	0.00	0.00	0.00	0.00	0.00	0.00	0.00	0.01	0.01	0.00	0.00
0.2	0.01	0.01	0.02	0.02	0.00	0.00	0.01	0.01	0.00	0.00	0.00	0.00
0.3	0.01	0.02	0.03	0.03	0.00	0.00	0.02	0.02	0.00	0.00	0.01	0.01
0.4	0.02	0.02	0.04	0.05	0.01	0.01	0.03	0.03	0.01	0.01	0.02	0.02
0.5	0.03	0.03	0.06	0.07	0.02	0.02	0.04	0.04	0.02	0.02	0.03	0.03
0.6	0.04	0.05	0.07	0.08	0.02	0.03	0.05	0.05	0.03	0.03	0.04	0.04
0.7	0.05	0.06	0.09	0.10	0.03	0.04	0.06	0.07	0.04	0.04	0.05	0.05
0.8	0.06	0.07	0.10	0.12	0.04	0.05	0.07	0.08	0.05	0.05	0.06	0.06
0.9	0.08	0.08	0.12	0.14	0.06	0.06	0.09	0.10	0.06	0.07	0.07	0.08

Such instances were seen in the remotely sensed data as widely varying pixel-level roof albedos within the boundaries of a roof, and were more likely to occur near the edges of flight strips. To ensure that roofs used for calibration had negligible specular reflection reaching the aerial sensor, we omitted buildings that (a) were near the flight strip edges, and (b) contained pixel-level albedos within the roof boundary that varied by more than 0.1.

2.6. Mean albedo for each roof

Mean albedos for each roof were calculated by averaging S' within each building outline. Some non-roofing materials were included since roofs can house HVAC equipment, skylights, solar photovoltaics, and other features. While we expect such equipment to minimally affect the mean roof albedo for each city, it can strongly affect the albedo of individual roofs. To estimate the magnitude of this effect, we used high-resolution imagery from USGS (see Section 2.3 and Fig. 3b) to compute the fraction of roof area covered by non-roof elements for 150 randomly selected buildings in Los Angeles. On average, non-roof elements were found to cover 2% of the footprint area for these roofs. Large buildings with low-slope roofs in many cases had a higher fractional coverage by non-roof elements, but these buildings make up a relatively small fraction of the total population of buildings in a city (see Ban-Weiss et al., 2015).

2.7. Precision of the remotely sensed albedos

As was mentioned in Section 2.1, about 30% of each city has overlapping imagery and therefore two values of remotely sensed roof albedo. For each city, duplicates were used to determine the precision error calculated as the scaled arithmetic difference,

$$\text{Scaled arithmetic difference} = \frac{(S'_2 - S'_1)}{\sqrt{2}} \quad (6)$$

where subscripts 1 and 2 index each duplicate value. Note that there is imprecision in each value S'_1 and S'_2; since these imprecisions add quadratically, we divide by $\sqrt{2}$ in Eq. (6) to determine the precision of one measurement (Hyslop and White, 2009). Each of the duplicates compares albedo computed using data obtained at two different view zenith angles ($-34°$ to $-30°$ versus $+30°$ to $+34°$) and solar zenith angles (see Section 2.1).

3. Results

3.1. Obtaining solar reflectance (broadband) from remotely sensed (narrowband) reflectances

We modeled $V = V(b, g, r)$ using the simple linear form:

$$V_k = c_b b_k + c_g g_k + c_r r_k \quad (7)$$

Here V_k, b_k, g_k, and r_k are band reflectances computed from Eq. (1); each c is a fitted coefficient; and subscript k indexes the 190 roofing samples. This linear model with $c_b = 0.37$, $c_g = 0.30$, and $c_r = 0.31$ predicts V with a coefficient of determination $R^2 = 0.99$. Fig. 5a evaluates the empirical model by comparing $V(b_k, g_k, r_k)$ to V_k. The minimal deviation of points from the one-to-one line indicates that the linear model well predicts V. A histogram of residuals (Fig. 5b) shows that the linear model can predict V to within 0.02; the root mean square (RMS) error χ is 0.003. Adding higher order terms and/or cross products to Eq. (7) did not improve the fit.

Next we attempted to quantify solar reflectance as:

$$S_k = c_b b_k + c_g g_k + c_r r_k + c_i i_k \quad (8)$$

The linear model with $c_b = 0.17$, $c_g = -0.13$, $c_r = 0.33$, and $c_i = 0.54$ predicts S with $R^2 = 0.99$. Fig. 5c evaluates the empirical model by comparing $S(b_k, g_k, r_k, i_k)$ to S_k. Again, there is minimal deviation from the one-to-one line, showing that the linear model well predicts S. More complicated variants to Eq. (8) were evaluated, this time including a

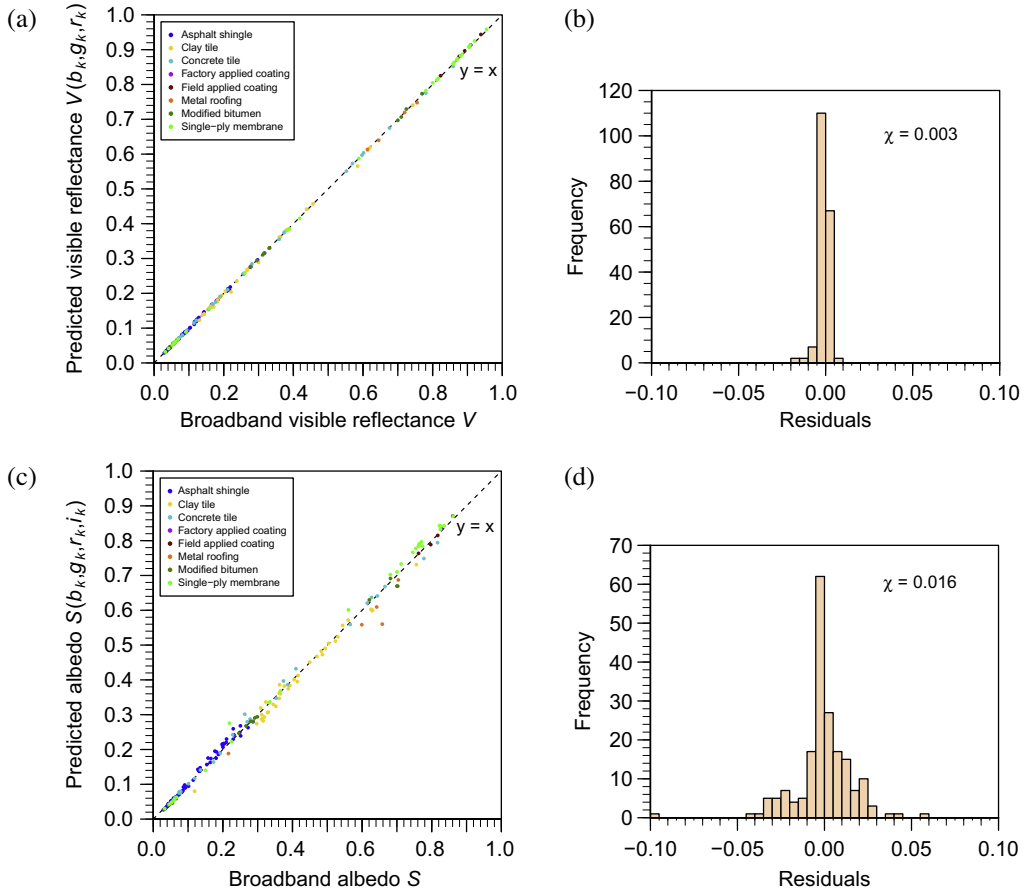

Fig. 5. Assessment of the empirical model for relating broadband reflectances to narrowband reflectances. All values are computed using solar spectral reflectance measurements of the 190 roof samples (Table 2). In (a) visible reflectance $V(b_k, g_k, r_k)$ computed using Eq. (7) is compared to V_k calculated from Eq. (1). The corresponding histogram of residuals is shown in (b). χ is the root mean square of the residuals. In (c), solar reflectance $S(b_k, g_k, r_k, i_k)$ computed using Eq. (8) is compared to S_k calculated from Eq. (1); the corresponding histogram of residuals is shown in (d).

term equal to the normalized difference vegetation index (NDVI).[2] The more complex models were found to be no better than the simple linear equation (Eq. (8)), whose histogram of residuals is shown in Fig. 5d. The linear model can predict S with an RMS error of 0.016.

The largest outlier is a metal roofing sample (zincalume with clear resin finish) in which $S(b_k, g_k, r_k, i_k)$ underpredicts S_k by 0.10. Fig. 4 shows the spectral reflectance of this outlier. It can be seen that the narrowband near-IR spectral range does not capture the increased reflectance at $\lambda > 1000$ nm; thus, i (833–920 nm) underpredicts broadband near-IR reflectance (700–2500 nm). A roofing product with strongly varying spectral reflectance in the near-IR may not always be well characterized by the narrowband near-IR reflectance i.

[2] NDVI is a metric that is often used to determine whether pixels contain live vegetation, and is calculated as $(I - V)/(I + V)$. Live vegetation characteristically has higher near-IR reflectance than visible reflectance, and therefore has NDVI > 0. The use of NDVI in this study was an attempt to identify cool roofs with low reflectance in the visible but high reflectance in the near-infrared. While the metric successfully identified cool colored roofs, adding it as a term to Eq. (8) did not improved the empirical model.

3.2. Calibrating remotely sensed values using ground truths

Fig. 6 shows measured versus remotely sensed (uncalibrated) albedos for the buildings that served as ground truths. Results for the City of Los Angeles and Long Beach are shown together since they are both part of the Greater Los Angeles Area. For low measured albedo ($S < 0.4$) most remotely sensed values are near measured values, while for high measured albedo ($S \geqslant 0.4$), the discrepancy is larger. Remotely sensed albedos are consistently lower than measured values. To derive remotely sensed (calibrated) albedos, the equations for each city shown in Fig. 6 were applied to the uncalibrated values.

Table 3 shows an estimate of the error (accuracy) at 90% confidence interval of the calibrated remotely sensed albedos. Error was calculated using Eqs. (4) and (5). Low albedo values are quite accurate, while high albedo values are generally less accurate. Note that the error for high albedo values is smaller in San Jose than in the other cities because we had a relatively high number ($N = 8$) of high albedo measurements, all of which had consistent remotely sensed values. The reported errors represent the estimated accuracy associated with the mean value for a given roof.

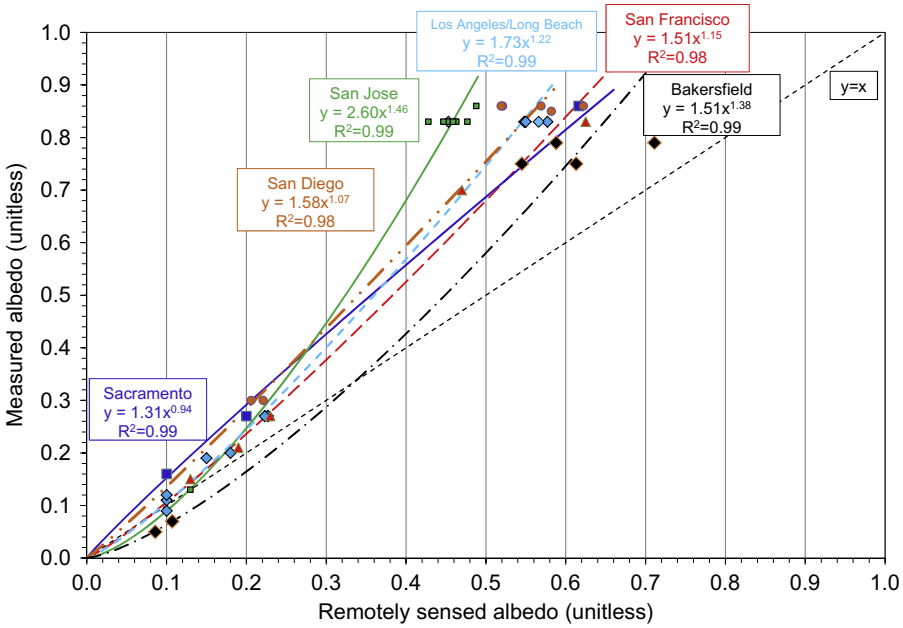

Fig. 6. Comparison of measured albedos (ground truths) to (uncalibrated) remotely sensed albedos. The equations shown were applied to the uncalibrated remotely sensed albedos $S(b_k, g_k, r_k, i_k)$ to compute calibrated values S' using Eq. (3). Coefficients of determination (R^2) for each power law fit are shown. Estimated errors for the calibrated remotely sensed albedos are in Table 3.

However, the relatively large error for high albedo roofs does not markedly influence the mean roof albedo for each city since high albedo roofs comprised a small fraction of total urban roof area in 2009. There may exist individual high albedo roofs that have errors larger than reported (i.e., outside the 90% confidence intervals) because of an increased contribution of specular reflectance. These outliers would most commonly have newly installed high albedo roofs with "curvy" roof shapes. The curves in the roof would mean that certain areas have high incidence angles and therefore significant specular reflectance (see Sections 2.5 and 4.1).

3.3. Maps of roof albedo

Fig. 7 shows a zoomed-in area of San Jose with the mean value of calibrated albedo S' for each roof. As expected in California due to Title 24 Building Energy Efficiency Standards (CEC, 2005), some commercial buildings with large flat roofs have high albedo. Homes with pitched roofs usually have low albedo roofs. Our companion paper (Ban-Weiss et al., 2015) shows city-wide results for all seven cities and provides further analysis.

4. Discussion and conclusions

4.1. Errors in computed albedo introduced by roof slope

In this study we do not account for the dependence of irradiance on roof slope. This simplification could lead to inaccuracies in remotely sensed albedo since it is the ratio of reflected to incident sunlight. We estimate the magnitude of the error from this simplification using results from Levinson et al. (2010) that quantify the dependence of typical clear-sky hemispherical (direct + diffuse) solar irradiance on roof pitch as a function of solar zenith angle (z). In Levinson et al., pitched roofs were approximated by the curved wall of a right circular cone since the population of pitched roof planes have no preferred azimuth orientation. In California, most pitched roofs have slope $\leqslant 23°$ (rise over run = 5:12), which we used as our pitched roof case for this error estimate.

Assuming $z = 0°$, hemispherical irradiance (I_h) on an axisymmetric surface with a 5:12 pitch is $I_h = 1030$ W m^{-2}, or 5.5% less than that on a horizontal surface ($I_h = 1090$ W m^{-2}). Assuming $z = 30°$, the maximum zenith angle during the flights that acquired the aerial imagery, I_h is 875 W m^{-2} for a roof pitch of 5:12, or 6.4% less than that on a horizontal surface ($I_h = 935$ W m^{-2}). Therefore, for $z \leqslant 30°$ we may have overestimated solar irradiance by up to about 6%, leading to underestimates for albedo of about 6%.

4.2. Precision error

The errors introduced by simplifications in viewing geometry (Section 2.2) and roof pitch (Section 4.1) used in this study can be explored by comparing the computed albedos derived for buildings that have overlapping imagery and therefore two remotely sensed values (see Section 2.7). Regions with duplicate albedos are generally at flight strip edges with corresponding view zenith angles of (a) −34° to −30°, and (b) +30° to +34°. Solar zenith angles also generally vary for each of the duplicate values,

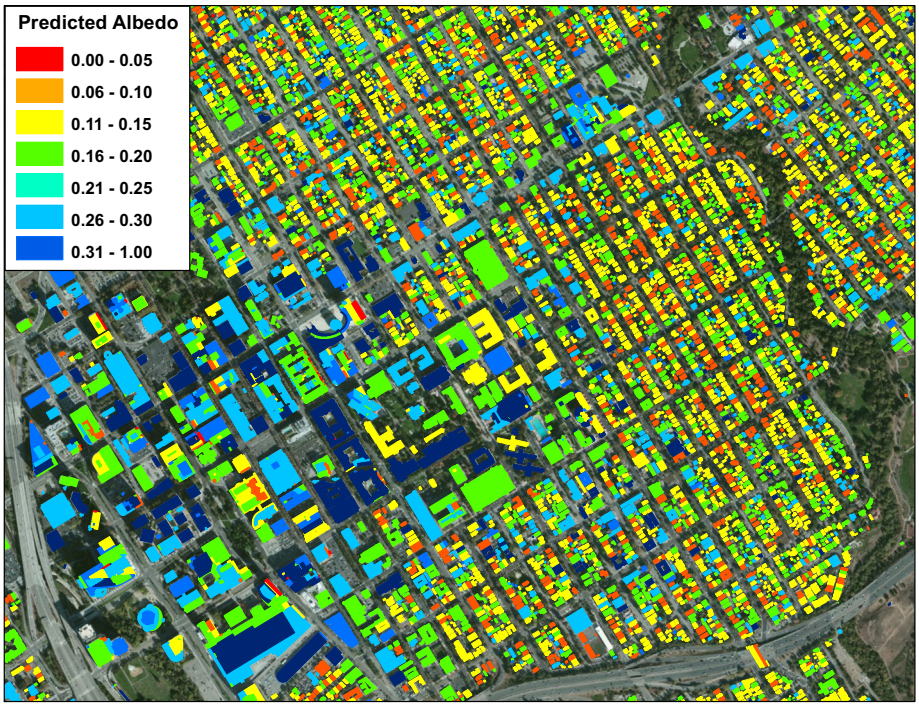

Fig. 7. A portion of San Jose showing the mean (calibrated) remotely sensed albedo for each rooftop. Albedos correspond to estimated bihemispherical solar reflectance.

though there is no consistent difference among flight strips. If the aforementioned simplifications introduced appreciable error, one would expect the duplicate remotely sensed albedos for a given building to be markedly different. The full precision analysis is presented in the companion paper (Ban-Weiss et al., 2015), but as an example result for one of the cities investigated here, the 430,332 buildings in Los Angeles with independently computed duplicate albedos showed an RMS scaled arithmetic difference (Eq. (6)) of 0.02, suggesting the simplifications discussed here lead to small errors for most roofs.

4.3. Summary

In this paper we have presented a method for deriving the mean albedo of individual roofs in California using aerial imagery (Fig. 1). The imagery (Fig. 2) was acquired on an airplane at high spatial resolution (1 m) in four spectral bands (three in the visible and one in the near-IR) using a radiometrically calibrated sensor. Including the near-IR band is important for quantifying roof albedo since (1) some "cool roofs" have low reflectance in the visible but high reflectance in the near-IR, and (2) about 50% of the energy from the sun is in the near-IR part of the solar spectrum. We have developed methods for (a) identifying building outlines (Table 1, Fig. 3), (b) converting the four narrowband reflectances to solar reflectance (albedo) based on laboratory measurements of solar spectral reflectance for 190 roofing products (Table 2, Figs. 4 and 5), and (c) calibrating remotely sensed albedos by comparing them to measured albedos of several roofs in each city (Fig. 6). We have found our method to be quite accurate for most roof types in California, though errors in computed albedos are relatively large for high albedo roofs that are presumably new and white (see Table 3). For example, roofs with an albedo near 0.2 had estimated errors (one-sided, 90% confidence intervals) ranging from 0 to 0.02, varying by city. On the other hand, roofs with an albedo near 0.8 had corresponding errors ranging from 0.05 to 0.12. The method was also shown to be precise. Precision error, computed using duplicate albedo values for roofs in flight overlap areas, was found to be 0.02 for Los Angeles (see Section 4.2). Each duplicate albedo was derived using remotely sensed data with differing viewing and illumination geometries.

In our companion paper (Ban-Weiss et al., 2015), we present city-wide albedo results for our seven California cities of interest, report results of the precision analysis for all analyzed cities, and provide additional analyses based on the city-wide results. We also use the roof albedo results for Bakersfield as an input to a regional climate model to predict the summer and winter temperature and precipitation changes that could result from converting the current stock of roofs to cool roofs.

Acknowledgements

The authors thank Ash Lashgari, Eileen McCauley, and Tony VanCuren of the California Air Resources Board; Doug Cain of North West Group; Sharon Chen, Pablo Rosado, Ben Mandel, and Ling Jin of Lawrence Berkeley National Laboratory; and Ana Paula Werle of Universidade de São Paulo. For rooftop access we thank John Skyberg and Christopher Brown of San Jose State

University; Leroy Sisneros and Fran Knight of University of California, Los Angeles; Chet Galland of California State University, Northridge; Craig Meyer of Pierce College; Victor Lai and Charles A. Meyer of San Francisco State University; and John Zertuche, Cynthia Kranc, and Jon Wildberger of University of California, Davis. For roof installation data we thank CertainTeed; Joe Mellott, Tom Chapman, Amy Digby, and Sean Gavin of The Garland Company, Inc.; Michael Kearney of GAF; Tony Zaffuto of Sylvester Roofing Co. Inc.; and Emmie Limon of SureCoat Systems. This project was funded by the California Air Resources Board under Contract 10-321. It was also supported by the Assistant Secretary for Energy Efficiency and Renewable Energy, Office of Building Technology, State, and Community Programs, of the U.S. Department of Energy under Contract No. DE-AC02-05CH11231. The statements and conclusions in this paper are those of the authors and not necessarily those of the California Air Resources Board.

References

Akbari, H., 2003. Measured energy savings from the application of reflective roofs in two small non-residential buildings. Energy 28, 953–967.

Akbari, H., Matthews, H.D., 2012. Global cooling updates: reflective roofs and pavements. Energy Build. 55, 2–6. http://dx.doi.org/10.1016/j.enbuild.2012.02.055.

Akbari, H., Rose, L.S., 2001a. Characterizing the fabric of the urban environment: a case study of metropolitan Chicago, Illinois. Lawrence Berkeley National Laboratory Report LBNL-49275, Berkeley, CA. <http://repositories.cdlib.org/lbnl/LBNL-49275>.

Akbari, H., Rose, L.S., 2001b. Characterizing the fabric of the urban environment: a case study of Salt Lake City, Utah. Lawrence Berkeley National Laboratory Report LBNL-47851, Berkeley, CA. <http://escholarship.org/uc/item/0wk718sm>.

Akbari, H., Rose, L.S., 2008. Urban surfaces and heat island mitigation potentials. J. Hum. – Environ. Syst. 11, 85–101.

Akbari, H., Rosenfeld, A., Taha, H., 1990. Summer heat islands, urban trees, and white surfaces. In: Proceedings of the 1990 ASHRAE Winter Conference. <http://isswprod.lbl.gov/library/view-docs/public/output/LBL-28308.pdf>.

Akbari, H., Davis, S., Dorsano, S., Huang, J., 1992. Cooling our communities: a guidebook on tree planting and light-colored surfacing. United States Environmental Protection Agency. Report number 22P.2001. <http://escholarship.org/uc/item/98z8p10x>.

Akbari, H., Bretz, S., Taha, H., Kurn, D., Hanford, J., 1997. Peak power and cooling energy savings of high-albedo roofs. Energy Build. 25, 117–126.

Akbari, H., Rose, L.S., Taha, H., 1999. Characterizing the fabric of the urban environment: a case study of Sacramento, California. Lawrence Berkeley National Laboratory Report LBNL-44688, Berkeley, CA. http://dx.doi.org/10.2172/764362.

Akbari, H., Pomerantz, M., Taha, H., 2001. Cool surfaces and shade trees to reduce energy use and improve air quality in urban areas. Sol. Energy 70, 295–310.

Akbari, H., Rose, L.S., Taha, H., 2003. Analyzing the land cover of an urban environment using high-resolution orthophotos. Landscape Urban Plann. 63, 1–14.

Akbari, H., Levinson, R., Rainer, L., 2005. Monitoring the energy-use effects of cool roofs on California commercial buildings. Energy Build. 37, 1007–1016.

Akbari, H., Menon, S., Rosenfeld, A., 2009. Global cooling: increasing world-wide urban albedos to offset CO_2. Climatic Change 94, 275–286.

Akbari, H., Matthews, H.D., Seto, D., 2012. The long-term effect of increasing the albedo of urban areas. Environ. Res. Lett. 7, 1–10.

ASTM, 2010. ASTM Standard C1549-09: Standard Test Method for Determining Solar Reflectance Near Ambient Temperature Using a Portable Solar Reflectometer. American Society for Testing and Materials, West Conshohocken, PA, <http://www.astm.org/Standards/C1549.htm>.

Ban-Weiss, G.A., Wray, C., Delp, W., Ly, P., Akbari, H., Levinson, R., 2013. Electricity production and cooling energy savings from installation of a building-integrated photovoltaic roof on an office building. Energy Build. 56, 210–220.

Ban-Weiss, G.A., Woods, J., Millstein, D., Levinson, R., 2015. Using remote sensing to quantify albedo of roofs in California's seven largest cities, Part 2: Results and application to climate modeling. Sol. Energy.

Beisl, U., Adiguezel, M., 2010. Validation of the reflectance calibration of the ADS40 airborne sensor using ground reflectance measurements. In: ISPRS TC VII Symposium – 100 Years ISPRS, Vienna, Austria, July 5–7, 2010, IAPRS, Vol. XXXVIII, Part 7B. <http://www.isprs.org/proceedings/XXXVIII/part7/b/pdf/80_XXXVIII-part7B.pdf>.

Beisl, U., Telaar, J., Schönermark, M.V., 2008. Atmospheric correction, reflectance calibration and BRDF correction for ADS40 image data. In: The International Archives of the Photogrammetry, Remote Sensing and Spatial Information Sciences, Vol. XXXVII, Part B7. <http://isprsserv.ifp.uni-stuttgart.de/proceedings/XXXVII/congress/7_pdf/1_WG-VII-1/02.pdf>.

Campra, P., Garcia, M., Canton, Y., Palacios-Orueta, A., 2008. Surface temperature cooling trends and negative radiative forcing due to land use change toward greenhouse farming in southeastern Spain. J. Geophys. Res. 113, D18109. http://dx.doi.org/10.1029/2008JD009912.

CEC, 2005. California Energy Commission Building Energy Efficiency Standards, For Residential and Nonresidential. Publication # CEC-400-2006-015. <http://www.energy.ca.gov/2006publications/CEC-400-2006-015/CEC-400-2006-015.PDF>.

City and County of San Francisco, 2011. San Francisco Data. Building Footprints. Obtained in 2011 at <https://data.sfgov.org>.

City of Bakersfield, 2011. Geographic Information Services. Obtained in 2011 at <http://www.bakersfieldcity.us/gis/downloads>.

City of San Jose, 2011. GIS/Public Works. Building outlines for 2006. Obtained in 2011 through personal communication with Vicky Gallardo, Senior Geosystems Specialist.

Cotana, F., Rossi, F., Filipponi, M., Coccia, V., Pisello, A.L., Bonamente, E., Petrozzi, A., Cavalaglio, G., 2014. Albedo control as an effective strategy to tackle global warming: a case study. Appl. Energy 130, 641–647. http://dx.doi.org/10.1016/j.apenergy.2014.02.065.

CRRC, 2013. Cool Roof Rating Council Rated Products Directory. <http://coolroofs.org>.

Downey, M., Uebbing, R., Gehrke, S., Beisl, U., 2010. Radiometric processing of ADS imagery: using atmospheric and BRDF corrections in products. In: ASPRS 2010 Annual Conference, San Diego, CA. <http://www.asprs.org/a/publications/proceedings/sandiego2010/sandiego10/Downey.pdf>.

Fraser, R.S., Ferrare, R.A., Kaufman, Y.J., Markham, B.L., Mattoo, S., 1992. Algorithm for atmospheric corrections of aircraft and satellite imagery. Int. J. Remote Sens. 13, 541–557.

Georgescu, M., Mahalov, A., Moustaoui, M., 2012. Seasonal hydroclimatic impacts of sun corridor expansion. Environ. Res. Lett. 7, 1–9.

Hyslop, N.P., White, W.H., 2009. Estimating precision using duplicate measurements. J. Air Waste Manage. Assoc. 59, 1032–1039. http://dx.doi.org/10.3155/1047-3289.59.9.1032.

Jacobson, M.Z., Ten Hoeve, J.E., 2012. Effects of urban surfaces and white roofs on global and regional climate. J. Clim. 25, 1028–1044.

Kaufman, J.Y., Sendra, C., 1988. Algorithm for automatic atmospheric corrections to visible and near-IR satellite imagery. Int. J. Remote Sens. 9, 1357–1381.

Konopacki, S., Akbari, H., 2001. Measured energy savings and demand reduction from a reflective roof membrane on a large retail store in Austin. Lawrence Berkeley National Laboratory Report LBNL-47149, Berkeley, CA. http://dx.doi.org/10.2172/787107.

Leica, 2013. Leica ADS80 Airborne Digital Sensor Digital Airborne Imaging Solution. <http://www.leica-geosystems.com/downloads123/zz/airborne/ads80/brochures-datasheet/ADS80_datasheet_en.pdf>.

Levinson, R., Akbari, H., 2010. Potential benefits of cool roofs on commercial buildings: conserving energy, saving money, and reducing emission of greenhouse gases and air pollutants. Energy Efficiency 3, 53–109.

Levinson, R., Berdahl, P., Abkari, H., Miller, W., Joedicke, I., Reilly, J., Suzuki, Y., Vondran, M., 2007. Methods of creating solar-reflective nonwhite surfaces and their application to residential roofing materials. Sol. Energy Mater. Sol. Cells 91, 304–314.

Levinson, R., Akbari, H., Berdahl, P., 2010. Measuring solar reflectance—Part I: Defining a metric that accurately predicts solar heat gain. Sol. Energy 84, 1717–1744.

Los Angeles Region Imagery Acquisition Consortium 3, 2011. LARIAC3. <http://planning.lacounty.gov/LARIAC/lariac3Main.htm>.

Lynn, B.H., Carlson, T.N., Rosenzweig, C., Goldberg, R., Druyan, L., Cox, J., Gaffin, S., Parshall, L., Civerolo, K., 2009. A modification to the NOAH LSM to simulate heat mitigation strategies in the New York City metropolitan area. J. Appl. Meteorol. Climatol. 48, 199–216.

Mackey, C.W., Lee, X., Smith, R.B., 2012. Remotely sensing the cooling effects of city scale efforts to reduce urban heat island. Build. Environ. 49, 348–358.

Markelin, L., Honkavaara, E., Beisl, U., Korpela, I., 2010. Validation of the radiometric processing chain of the LEICA ADS40 airborne photogrammetric sensor. In: ISPRS TC VII Symposium – 100 Years ISPRS, Vienna, Austria, July 5–7, 2010, IAPRS, Vol. XXXVIII, Part 7A. <http://www.isprs.org/proceedings/XXXVIII/part7/a/pdf/145_XXXVIII-part7A.pdf>.

Menon, S., Akbari, H., Mahanama, S., Sednev, I., Levinson, R., 2010. Radiative forcing and temperature response to changes in urban albedos and associated CO_2 offsets. Environ. Res. Lett. 5, 1–11.

Millstein, D., Menon, S., 2011. Regional climate consequences of large-scale cool roof and photovoltaic array deployment. Environ. Res. Lett. 6, 1–9.

NAIP, 2013. National Agriculture Imagery Program, United States Department of Agriculture's Farm Service Agency (FSA). <http://www.fsa.usda.gov/FSA/apfoapp?area=home&subject=prog&topic=nai>.

Nilson, T., Kuusk, A., 1989. A reflectance model for the homogeneous plant canopy and its inversion. Remote Sens. Environ. 27, 157–167.

Oleson, K.W., Bonan, G.B., Feddema, J., 2010. Effects of white roofs on urban temperature in a global climate model. Geophys. Res. Lett. 37. http://dx.doi.org/10.1029/2009GL042194.

Parker, D.S., Barkaszi Jr., S.F., Chandra, S., Beal, D.J., 1995. Measured cooling energy savings from reflective roofing systems in Florida: field and laboratory research results. In: Proceedings of the Thermal Performance of the Exterior Envelopes of Buildings VI, Clearwater, FL, December 4–8.

Parker, D.S., Sherwin, J.R., Sonne, J.K., 1998. Measured performance of reflective roofing systems in a Florida commercial building. Am. Soc. Heating Refrig. Air Cond. Eng., Atlanta, Georgia, January, ASHRAE Trans. 104, 1.

Rose, L.S., Akbari, H., Taha, H., 2003. Characterizing the fabric of the urban environment: a case study of greater Houston, Texas. Lawrence Berkeley National Laboratory Report LBNL-51448, Berkeley, CA. <http://repositories.cdlib.org/lbnl/LBNL-51448>.

Rosenfeld, A., Akbari, H., Bretz, S., Fishman, B., Kurn, D., Sailor, D., Taha, H., 1995. Mitigation of urban heat islands: materials, utility programs, updates. Energy Build. 22, 255–265.

Schaaf, C.B., 2004. MODIS BRDF/Albedo Product (MOD43B) User's Guide. http://www-modis.bu.edu/brdf/userguide/albedo.html>. See also <http://modis-atmos.gsfc.nasa.gov/ALBEDO>.

Schaaf, C.B., Gao, F., Strahler, A.H., Lucht, W., Li, X.W., Tsang, T., et al., 2002. First operational BRDF, albedo nadir reflectance products from MODIS. Remote Sens. Environ. 83, 135–148.

Schaepman-Strub, G., Schaepman, M.E., Painter, T.H., Dangel, S., Martonchik, J.V., 2006. Reflectance quantities in optical remote sensing – definitions and case studies. Remote Sens. Environ. 103, 27–42.

Slaton, M.R., Hunt Jr., E.R., Smith, W.K., 2001. Estimating near-infrared leaf reflectance. Am. J. Bot. 88, 278–284.

Sleiman, M., Ban-Weiss, G.A., Gilbert, H., Francois, D., Berdahl, P., Kirchstetter, T., Destaillats, H., Levinson, R., 2011. Soiling of building envelope surfaces and its effect on solar reflectance – Part I: Analysis of roofing product databases. Sol. Energy Mater. Sol. Cells 95, 3385–3399.

Song, J., Lu, D., Weseley, M.L., 2003. A simplified atmospheric correction procedure for the normalized difference vegetation index. Photogramm. Eng. Remote Sens. 69, 521–528.

Synnefa, A., Dandou, A., Santamouris, M., Tombrou, M., Soulakellis, N., 2008. On the use of cool materials as a heat island mitigation strategy. J. Appl. Meteorol. Climatol. 47, 2846–2856.

Taha, H., 2008a. Urban surface modification as a potential ozone air-quality improvement strategy in California: a mesoscale modelling study. Boundary Layer Meteorol. 127, 219–239.

Taha, H., 2008b. Meso-urban meteorological and photochemical modeling of heat island mitigation. Atmos. Environ. 42, 8795–8809.

Taha, H., 2008c. Episodic performance and sensitivity of the urbanized MM5 (uMM5) to perturbations in surface properties in Houston Texas. Boundary Layer Meteorol. 127, 193–218.

Taha, H., Akbari, H., Rosenfeld, A., Huang, J., 1988. Residential cooling loads and the urban heat island—the effects of albedo. Build. Environ. 23, 271–283.

Wanner, W., Li, X., Strahler, A.H., 1995. On the derivation of kernels for kernel-driven models of bidirectional reflectance. J. Geophys. Res. 100, 21077–21089.

Zhou, Y., Shepherd, J.M., 2009. Atlanta's urban heat island under extreme heat conditions and potential mitigation strategies. Nat. Hazards 52, 639–668.